## ENHANCED DIFFUSIVITY AND SKEWNESS OF A DIFFUSING TRACER IN THE PRESENCE OF AN OSCILLATING WALL

LINGYUN DING \*, ROBERT HUNT \*, RICHARD M. MCLAUGHLIN\*†, AND HUNTER WOODIE \*

Abstract. We examine a passive scalar diffusing in time-varying flows which are induced by a periodically oscillating wall in a Newtonian fluid between two infinite parallel plates as well as in an infinitely long duct. These shear flows yield the generalized Ferry waves which are exact solutions of the Navier-Stokes equations. First, we calculate the second Aris moment for all time, and its long time limiting effective diffusivity as a function of the geometrical parameters, frequency, viscosity, and diffusivity. We show that the viscous dominated limit results in a linear shear layer for which the effective diffusivity is bounded with upper bound  $\kappa(1 + A^2/(2L^2))$ , where  $\kappa$  is the tracer diffusivity, A is the amplitude of oscillation, and L is the gap thickness. Alternatively, we show that for finite viscosities the enhanced diffusion is unbounded, diverging in the high frequency limit. Physical arguments are given to explain these striking differences. Asymptotics for the high frequency behavior as well as the low viscosity limit are computed. Study of the exact formula shows that a maximum exists as a function of the viscosity, suggesting a possible optimal temperature for mixing in this geometry. Physical experiments are performed in water using Particle Tracking Velocimetry to quantitatively measure the fluid flow. Using fluorescein dye as the passive tracer, we document that the theory is quantitatively accurate. Further, we show that the scalar skewness is zero for linear shear at all times, whereas for the nonlinear Ferry wave, using Monte-Carlo simulations, we show the skewness sign (as well as front versus back loaded distributions) can be controlled through the phase of the oscillating wall. Lastly, short time skewness asymptotics are computed for the Ferry wave and compared to the Monte-Carlo simulations.

Key words. Passive Scalar, Effective Diffusion, Skewness

1. Introduction. An extremely important class of problems concerns how fluid motion can increase solute mixing. Since G. I. Taylor first introduced the calculation showing that a pressure driven flow in a pipe leads to a hugely boosted effective diffusivity [21], the literature on this topic has exploded in many directions spanning many disciplines. The mathematics of this problem is particularly important and just one of the many areas of Modern Applied Mathematics which Andy Majda pioneered, starting with work on developing a rigorous formulation characterizing how a scale separated flow with general streamline topology can give rise to an effective diffusivity [5, 17] extending to non-scale separated flows showing anomalous results [6, 7, 8], and eventually yielding models of scalar intermittency [16, 18] which produced explicit models for the full PDF of a passive scalar advected by a random, white in time linear shear layer [11, 10, 22, 14, 22, 13]

Shortly following G. I. Taylor, Aris presented an alternative approach for shear layers yielding a hierarchy for the spatial moments of the scalar field. More recent results have explored how geometry can be used to control these moments to seek different effective diffusivities [20, 1], and even how geometry can be used to control how solute in pressure driven flow can be delivered with either a sharp front, or with a gradual build-up through a detailed study of the scalar skewness [3, 2].

Recently, Vedel and Bruus [23] explored the case of a time-varying shear layer in a pipe or channel and developed some interesting formulas which demonstrated that it is possible to obtain a boosted effective diffusivity over the bare molecular

<sup>\*</sup>Department of Mathematics, the University of North Carolina at Chapel Hill, 27599(dingly@live.unc.edu, huntrl@live.unc.edu, rmm@email.unc.edu, woodieh@live.unc.edu )

<sup>&</sup>lt;sup>†</sup>Corresponding author

diffusion through oscillatory flows in the absence of a pressure gradient (i.e. a flow not producing any net transport). Our study builds upon this by exploring a physically realizable flow induced by the oscillatory motion of a wall adjacent to a fluid. We first derive the solutions to the Navier-Stokes equations resulting from this motion, which was originally presented by Ferry [15, 19]. We see that in the high viscosity limit, this flow results in a time-varying linear shear layer. In turn, we compute the effective diffusivity produced by this flow and establish an upper bound for the case of a time-varying linear shear, showing the maximum possible diffusion is set by the amplitude of wall motion and the gap thickness of the channel and is independent of the frequency of motion. Alternatively, we demonstrate that, for finite viscosities, the effective diffusivity is unbounded in increasing frequency of wall motion. These results are validated with experiments performed using a wall driven by a programmable linear motor. Lastly, we prove that for the case of the time-varying linear shear layer, the scalar spatial skewness is zero for all time, while Monte-Carlo simulations for wall driven flows show that at finite viscosities the skewness can be non-zero. Short time asymptotics akin to prior work [3] are computed for the skewness and compared directly to the Monte-Carlo simulations.

2. Theoretical calculations. In this section, we first review the Aris moment hierarchy [4] for time-varying shear layers. We then compute the Ferry wave shear flows induced from a moving wall and compute the effective diffusivity as a function of the physical parameters.

**2.1.** Aris Moment Hierarchy: The advection-diffusion equation with general time-varying shear flow u(y, z, t) and no-flux boundary condition takes the form

(2.1) 
$$\begin{array}{rcl} \frac{\partial T}{\partial t} + u(y,z,t)\frac{\partial T}{\partial x} &= & \kappa \Delta T \\ \frac{\partial T}{\partial \mathbf{n}}|_{\partial \Omega} &= & 0 \\ T(x,y,z,0) &= & f(x,y,z) \end{array}$$

where  $\kappa$  is the diffusivity and f(x, y, z) is the initial data. The *n*th Aris moment is defined by  $T_n = \int_{-\infty}^{\infty} x^n T(x, y, z, t) dx$ . With the assumption  $T(\pm \infty, y, z, t) = 0$ , Aris moment satisfies the recursive relationship called Aris equation,

(2.2) 
$$\begin{array}{rcl} (\partial_t - \kappa \Delta)T_n &=& \kappa n(n-1)T_{n-2} + nu(y,z,t)T_{n-1} \\ \frac{\partial T_n}{\partial \mathbf{n}}|_{\partial \Omega} &=& 0 \\ T_n(y,z,0) &=& \int\limits_{-\infty}^{\infty} x^n f(x,y,z) \mathrm{d}x \end{array}$$

where  $T_{-1} = 0$ .

The full moments of T are then obtained though the cross-sectional average of the moments  $\langle T_n \rangle = \frac{1}{|\Omega|} \int_{\Omega} T_n dy dz$ , where  $\Omega$  is the cross section and  $|\Omega|$  is the area of  $\Omega$ . Applying the divergence theorem and boundary conditions gives

(2.3) 
$$\frac{\frac{\mathrm{d}\langle T_n \rangle}{\mathrm{d}t} = \kappa n(n-1) \langle T_{n-2} \rangle + n \langle u(y,z,t) T_{n-1} \rangle}{\langle T_n \rangle (0) = \frac{1}{|\Omega|} \int_{\Omega} \int_{-\infty}^{\infty} x^n f(x,y,z) \mathrm{d}x \mathrm{d}y \mathrm{d}z} }$$

In this paper, we focus on the channel domain, namely,  $\Omega = \{(x, y) | x \in \mathbb{R}, y \in [0, L]\}$  for two dimensional problem and  $\Omega = \{(x, y, z) | x, z \in \mathbb{R}, y \in [0, L]\}$  for three dimensional problem.

**2.2. Ferry shear wave.** We consider a layer of incompressible fluid between two infinite parallel walls with gap thickness L. The lower wall is stationary while the upper wall is moving periodically with the velocity f(t). The flow u(y,t) induced by the upper moving wall satisfies the equation

(2.4) 
$$\begin{aligned} u_t &= \nu u_{yy} \\ u(0,t) &= 0, \quad u(L,t) = f(t), u(y,0) = 0 \end{aligned}$$

where  $\nu$  is the fluid dynamic viscosity. The solution obtained by Laplace transform takes the form

(2.5) 
$$u(y,t) = \frac{1}{2\pi i} \int_{C-i\infty}^{C+i\infty} e^{st} \hat{f}(s) \frac{\sinh\left(\frac{s}{\nu}y\right)}{\sinh\left(\frac{s}{\nu}L\right)} ds$$

where  $\hat{f}(s)$  is the Laplace transformation of wall velocity f(t). Consider a harmonic motion of wall  $f(t) = A\omega \cos \omega t$ , the integrand in the equation (2.5) becomes

(2.6) 
$$e^{st}\hat{u}(y,s) = e^{st}\frac{As\omega}{s^2 + \omega^2}\frac{\sinh\left(\frac{s}{\nu}y\right)}{\sinh\left(\frac{s}{\nu}L\right)}$$

The poles of  $\hat{u}$  are  $\pm i\omega, -\frac{\pi^2 \nu n^2}{L^2}$  for  $n \in \mathbb{Z}^+$ . By the residue theorem, we have

We neglect the exponential decay term in the following calculation.

**2.3. Enhanced diffusivity induced by an oscillating wall.** In this section, we calculate the enhanced diffusivity induced by the Ferry wave. We take the strip function  $T(x, y, z, 0) = \delta(x)$  as initial data, so  $T_0(y, z, 0) = 1$  and  $T_n(y, z, 0) = 0$  for  $n \ge 1$ . Since the initial function and Ferry shear wave flow studied here are independent on z, the three dimensional advection-diffusion equation reduces to an equation in two spatial dimensions. We note that in the appendix we derive the generalized three dimensional Ferry wave solution.

When n = 0, the equation (2.1) is

(2.8)  
$$\begin{aligned} & (\partial_t - \kappa \Delta) T_0 = & 0\\ & \frac{\partial T_0}{\partial y}|_{y=0,L} = & 0\\ & T_0(y,0) = & 1\\ & 3 \end{aligned}$$

Clearly,  $T_0 = 1$ . When n = 1, the equation (2.1) is

(2.9) 
$$\begin{array}{rcl} (\partial_t - \kappa \Delta)T_1 &= & u(y,t)T_0\\ \frac{\partial T_1}{\partial y}|_{y=0,L} &= & 0\\ T_1(y,0) &= & 0 \end{array}$$

Based on the boundary condition, we choose  $\sqrt{\frac{1}{L}}, \sqrt{\frac{2}{L}} \cos i\pi \frac{y}{L}, i = 1, ...$  as the orthogonal basis. The solution of (2.9) obtained by series expansion takes the form:

(2.10) 
$$T_1 = \sum_{i=0}^{\infty} a_i(t) \cos i\pi \frac{y}{L}$$

When n = 2, the cross sectional average satisfies the equation

(2.11) 
$$\frac{\frac{\mathrm{d}\langle T_2 \rangle}{\mathrm{d}t}}{\langle T_2 \rangle(0) = 0} = 2\kappa \langle T_0 \rangle + 2 \langle u(y, z, t) T_1 \rangle$$

After integrating the right hand side of above equation, we have (2.12)

$$\langle T_2(t) \rangle = 2\kappa t - \sum_{i=1}^{\infty} \frac{2\pi^2 A^2 i^2 \kappa L^4 r^2 \left( (-1)^{2i} \left( \cos\left(\sqrt{2}Lr\right) + \cosh\left(\sqrt{2}Lr\right) \right) - 4(-1)^i \cos\left(\frac{Lr}{\sqrt{2}}\right) \cosh\left(\frac{Lr}{\sqrt{2}}\right) + 2 \right)}{(\pi^4 i^4 + L^4 r^4)(\pi^4 i^4 \kappa^2 + L^4 \omega^2) \left( \cos\left(\sqrt{2}Lr\right) - \cosh\left(\sqrt{2}Lr\right) \right)} t + O(1)$$

where we denote  $r = \sqrt{\frac{\omega}{\nu}}$  for simplicity. The effective diffusivity is then (2.13)

$$\begin{split} \kappa_{eff} &= \frac{\langle T_2 \rangle - \langle T_1 \rangle^2}{2t} = \\ \kappa + \frac{\kappa \pi^2 A^2 L^4 r^2}{\cosh(\sqrt{2}Lr) - \cos(\sqrt{2}Lr)} \left( -\frac{\sin(\sqrt{2}Lr) + \sinh(\sqrt{2}Lr)}{2\sqrt{2}\pi^2 L^5(\kappa^2 r^5 - r\omega^2)} \right. \\ &+ \frac{\kappa \pi^2 A^2 L^4 r^2}{2\sqrt{2}\pi^2 L^5 \sqrt{\omega}(\cos(\sqrt{2}Lr) - 1)(\cosh(\sqrt{2}Lr) - 1)(\omega^2 - \kappa^2 r^4) \left(\cos\left(\frac{\sqrt{2}L\sqrt{\omega}}{\sqrt{\kappa}}\right) - \cosh\left(\frac{\sqrt{2}L\sqrt{\omega}}{\sqrt{\kappa}}\right)\right)} \times \\ &\left( -2\sin\left(\frac{L\sqrt{2}\omega}{\sqrt{\kappa}}\right) + \cos^2\left(\sqrt{2}Lr\right)\sin\left(\frac{L\sqrt{2}\omega}{\sqrt{\kappa}}\right) + \cos\left(\sqrt{2}Lr\right)\sin\left(\frac{L\sqrt{2}\omega}{\sqrt{\kappa}}\right) \\ &- 8\sin\left(\frac{Lr}{\sqrt{2}}\right)\sin\left(\sqrt{2}Lr\right)\sinh\left(\frac{Lr}{\sqrt{2}}\right)\sinh\left(\sqrt{2}Lr\right)\sin\left(\frac{L\sqrt{\omega}}{\sqrt{2}\kappa}\right)\cosh\left(\frac{L\sqrt{\omega}}{\sqrt{2}\kappa}\right) \\ &+ 8\sin\left(\frac{Lr}{\sqrt{2}}\right)\sin\left(\sqrt{2}Lr\right)\sinh\left(\frac{Lr}{\sqrt{2}}\right)\sinh\left(\sqrt{2}Lr\right)\cos\left(\frac{L\sqrt{2}\omega}{\sqrt{2}}\right)\sinh\left(\frac{L\sqrt{\omega}}{\sqrt{2}\kappa}\right) \\ &+ 2\sin^2\left(\frac{Lr}{\sqrt{2}}\right)\cosh^2\left(\sqrt{2}Lr\right)\left(\sin\left(\frac{L\sqrt{2}\omega}{\sqrt{\kappa}}\right) - \sinh\left(\frac{L\sqrt{2}\omega}{\sqrt{\kappa}}\right)\right) \\ &+ 2\sin^2\left(\frac{Lr}{\sqrt{2}}\right)\left(\cos\left(\sqrt{2}Lr\right) + 2\right)\sinh\left(\frac{L\sqrt{2}\omega}{\sqrt{\kappa}}\right) + O\left(\frac{1}{t}\right) \end{split}$$

When  $\nu \to \infty$ , the Ferry shear wave converges to the linear shear flow  $u(y,t) = \frac{Ay\omega \sin \omega t}{L}$ . In the high viscosity limit, the effective diffusivity (2.13) becomes

(2.14) 
$$\kappa_{eff} = \kappa \left( 1 + \frac{A^2 \left( L\sqrt{\omega} - \frac{\sqrt{2}\sqrt{\kappa} \left( \sin\left(\frac{L\sqrt{\omega}}{\sqrt{2\kappa}}\right) + \sinh\left(\frac{L\sqrt{\omega}}{\sqrt{2\kappa}}\right) \right)}{\cos\left(\frac{L\sqrt{\omega}}{\sqrt{2\kappa}}\right) + \cosh\left(\frac{L\sqrt{\omega}}{\sqrt{2\kappa}}\right)} \right)}{2L^3\sqrt{\omega}} \right) \\ \leq \kappa (1 + \frac{A^2}{2L^2})$$

which is bounded by a constant set solely by the gap thickness and the amplitude of wall motion. Alternatively, in Ferry wave case at finite viscosities, the effective

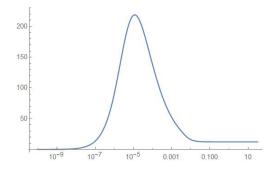


FIG. 1. The ratio  $\frac{\kappa_{eff} - \kappa}{\kappa}$  versus the viscosity for parameters  $\omega = 1/s$ , L = 0.2cm, A = 1cm,  $\kappa = 5 * 10^{-6} cm^2/s$ .

diffusivity is unbounded in the high frequency limit. In fact, we have the following asymptotic expansion in high frequency:

(2.15) 
$$\kappa_{eff} \sim \kappa \left(1 + \frac{A^2 \nu \sqrt{\omega}}{2\sqrt{2}L\left(\sqrt{\kappa} + \sqrt{\nu}\right)(\kappa + \nu)}\right), \quad \omega \to \infty$$

We also can compute the asymptotics in the low viscosity limit,  $\nu \to 0^+$  which yields:

(2.16) 
$$\kappa_{eff} \sim \kappa \left( 1 + \frac{A^2 \nu \sqrt{\omega} \left( \sin \left( \frac{\sqrt{2}L \sqrt{\omega}}{\sqrt{\kappa}} \right) - \sinh \left( \frac{\sqrt{2}L \sqrt{\omega}}{\sqrt{\kappa}} \right) \right)}{2\sqrt{2} \kappa^{3/2} L \left( \cos \left( \frac{\sqrt{2}L \sqrt{\omega}}{\sqrt{\kappa}} \right) - \cosh \left( \frac{\sqrt{2}L \sqrt{\omega}}{\sqrt{\kappa}} \right) \right)} \right)$$

Of course, since no fluid motion is generated for a parallel wall moving in an ideal fluid, the boosted diffusivity vanishes in this limit. This implies potential existence of a maximum effective diffusivity as the viscosity is varied. To demonstrate this, we plot in figure 1 the normalized enhanced diffusivity as a function of the fluid viscosity with parameters  $\omega = 1/s$ , L = 0.2 cm, A = 1 cm,  $\kappa = 5 * 10^{-6}$  cm<sup>2</sup>/s. Since, for instance, the fluid viscosity and diffusivity are functions of temperature, this could provide a recipe for optimal mixing.

2.4. Enhanced diffusivity for linear shear flow with general periodic wall motion. Suppose the position of wall is a general mean zero periodic function of time,  $F(\omega t)$ . In the high viscosity limit, the induced velocity is  $u(y,t) = \frac{y\omega f(\omega t)}{L}$ , where f is the derivative of F. The centered cross sectional average, e.g., variance and skewness, is invariant under the galilean transformation  $\tilde{x} = x - ut$ , where u is a constant. We consider the problem in a frame of reference moving with the spatial mean speed, so the velocity becomes:

(2.17) 
$$u(y,t) = \frac{(y-\frac{L}{2})\omega f(t)}{L} = -\frac{4\omega f(t)}{\pi^2} \sum_{i \in \text{odd}}^{\infty} \frac{\cos i\pi \frac{y}{L}}{i^2}$$

Solving (2.9) with velocity (2.17), we have

(2.18) 
$$T_1(y,t) = -\sum_{i,odd}^{\infty} e^{-\frac{\pi^2 i^2 \kappa t}{L^2}} \int_0^t \frac{4e^{\frac{i^2 \pi^2 \kappa s}{L^2}} \omega f(\omega s)}{i^2 \pi^2} ds \cos i\pi \frac{y}{L}$$

Substitute (2.18) into (2.3) leads to

(2.19) 
$$\frac{\frac{\mathrm{d}\langle T_2 \rangle}{\mathrm{d}t} = 2\kappa \langle T_0 \rangle + 2\left\langle \frac{(y-\frac{L}{2})\omega f(t)}{L} T_1 \right\rangle}{= 2\kappa + f(\omega t) \sum_{i,odd}^{\infty} \frac{4\omega}{\pi^2 i^2} e^{-\frac{\pi^2 i^2 \kappa t}{L^2}} \int_0^t \frac{4e^{\frac{i^2 \pi^2 \kappa s}{L^2}} \omega f(\omega s)}{i^2 \pi^2} ds$$

After a straightforward calculation, we have

(2.20) 
$$\langle T_2 \rangle (t) = 2\kappa t + \sum_{i,odd}^{\infty} \left(\frac{4\omega}{\pi^2 i^2}\right)^2 \int_0^t e^{-\frac{\pi^2 i^2 \kappa \tau}{L^2}} f(\omega \tau) \int_0^\tau e^{\frac{i^2 \pi^2 \kappa s}{L^2}} f(\omega s) ds d\tau$$

Using the Fourier series expansion  $f(t) = \sum_{k=1}^{\infty} A_k \sin kt + B_k \cos kt$ , we have

(2.21) 
$$\langle T_2 \rangle (t) = 2\kappa t + \sum_{i,odd}^{\infty} \left(\frac{4\omega}{\pi^2 i^2}\right)^2 \left(\sum_{k=1}^{\infty} \frac{(A_k^2 + B_k^2)\pi^2 i^2 \kappa L^2}{2\pi^4 i^4 \kappa^2 + 2k^2 L^4 \omega^2}\right) t + O(1)$$

The effective diffusivity is then: (2.22)

$$\begin{split} \kappa_{eff} &= \frac{\langle T_2 \rangle(t)}{2t} = \kappa + \frac{\kappa}{2} \sum_{i,odd}^{\infty} \left(\frac{4\omega}{\pi^{2}i^2}\right)^2 \left(\sum_{k=1}^{\infty} \frac{\left(A_k^2 + B_k^2\right) \pi^2 i^2 L^2}{2\pi^4 i^4 \kappa^2 + 2k^2 L^4 \omega^2}\right) + O\left(\frac{1}{t}\right) \\ &= \kappa + \frac{\kappa}{2} \sum_{k=1}^{\infty} \left(A_k^2 + B_k^2\right) \left(\frac{1}{k^2 L^2} + \frac{\sqrt{\kappa} \left(-\frac{\sqrt{2} \sin\left(\frac{\sqrt{k} L \sqrt{\omega}}{\sqrt{2} \sqrt{\kappa}}\right)}{\cos\left(\frac{\sqrt{k} L \sqrt{\omega}}{\sqrt{2} \sqrt{\kappa}}\right) + \cosh\left(\frac{\sqrt{k} L \sqrt{\omega}}{\sqrt{2} \sqrt{\kappa}}\right)} - \frac{\sqrt{2} \sinh\left(\frac{\sqrt{k} L \sqrt{\omega}}{\sqrt{2} \sqrt{\kappa}}\right)}{\cos\left(\frac{\sqrt{k} L \sqrt{\omega}}{\sqrt{2} \sqrt{\kappa}}\right) + \cosh\left(\frac{\sqrt{k} L \sqrt{\omega}}{\sqrt{2} \sqrt{\kappa}}\right) + \cos\left(\frac{\sqrt{k} L \sqrt{\omega}}{\sqrt{2} \sqrt{\kappa}}\right)}\right)}\right) + O\left(\frac{1}{t}\right) \end{split}$$

We again can find an upper bound for the enhanced diffusivity:

(2.23) 
$$\kappa_{eff} \leq \kappa \left(1 + \frac{1}{2L^2} \sum_{k=1}^{\infty} \frac{A_k^2 + B_k^2}{k^2}\right)$$

When  $f(t) = A\omega \sin(\omega t)$ , the bound in (2.23) reduce to the bound in (2.14).

2.5. Zero Skewness for linear shear and Geometric Skewness for nonlinear Ferry-wave. First, it is fairly straightforward to show that the passive scalar skewness is generally zero for any linear shear flow for delta function initial data independent of y with a temporally periodic wall motion because of the different parity of the cosine expansions. Observe that the linear shear admits an odd cosine expansion in y and produces an odd  $T_1$  cosine expansion in y. In turn, we see that  $T_2$  is even from inspection, since the driver in the equation for  $T_2$  is the product of two functions u and  $T_1$  which are odd about y = L/2. Lastly, the driver for the  $T_3$  equation contains  $T_1$  (odd) and the product of u (odd) and  $T_2$  (even). When computing the net third moment by cross-sectional averaging,  $< T_1 >= 0$  as well as  $< uT_2 >= 0$ . Hence, the skewness is zero for a linear shear. We note below using computational simulations that the skewness for the more general Ferry wave is non-zero.

Second, by neglecting the molecular diffusion, the method of characteristics can be utilized to compute what is called the geometric skewness [3], which leads to the short time asymptotic expansion of the skewness with diffusion present. For the initial function f(x, y), the solution can be obtained by method of characteristics as  $T(x, y, t) = f(x - \int_{0}^{t} u(y, s) ds, y, t)$ . The cross sectional average of N-th Aris moment is  $\langle T_n \rangle = \frac{1}{L} \int_{-\infty}^{\infty} x^n dx \int_0^L dy f(x - \int_0^t u(y, s) ds, y, t)$ . This leads to a lengthy analytical formula for the geometric skewness,  $\frac{\langle T_3 \rangle - 3 \langle T_2 \rangle \langle T_1 \rangle + 2 \langle T_1 \rangle^3}{(\langle T_2 \rangle - \langle T_1 \rangle^2)^{\frac{3}{2}}}$ , which is too long to list here. We will study its behavior in section 5 and compare with computational simulations.

**3.** Computational approaches. Here we describe the two computational approaches we utilize to solve the advection-diffusion equation.

First, we utilize Monte-Carlo simulations. The Monte-Carlo simulations are used to compare with the laboratory experiments described in the following section. To get a global approximation of the solution of the advection-diffusion equation, we adopt the forward Monte-Carlo method. We determine the initial position of 10<sup>7</sup> particles according to the intensity distribution of the photo from the experiment on a uniform grid. Each particle's trajectory satisfies the stochastic differential equation(SDE),

(3.1)  
$$dX_t = u(Y_t, t)dt + \sqrt{2\kappa}dW_1$$
$$dY_t = \sqrt{2\kappa}dW_2$$
$$dZ_t = \sqrt{2\kappa}dW_3$$

where u(y,t) is the Ferry wave,  $\kappa$  is diffusivity and  $dW_i$  are independent white noises. We solve the SDE by Euler scheme with a time increment  $\Delta t = 0.05$ .

(3.2) 
$$X_{t_{i+1}} = X_{t_i} + u(Y_{t_i}, t_i)\Delta t + \sqrt{2\kappa\Delta t}n_{i,1}$$
$$Y_{t_{i+1}} = Y_{t_i} + \sqrt{2\kappa\Delta t}n_{i,2}$$
$$Z_{t_{i+1}} = Z_{t_i} + \sqrt{2\kappa\Delta t}n_{i,3}$$

 $n_{i,j}$  are independent and identically distributed standard normal random variables which are produced by the Mersenne Twister algorithm and uniform random number generator. We impose the billiard-like reflection rules on the boundary plane z = 0, z = 16, y = 0, y = 0.16. At a given time t, the histogram of the  $10^7$  particle positions is an approximation of the solution T(x, y, z, t). The cross sectional average of N-th Aris moment can be approximated by the formula

(3.3) 
$$\langle T_n \rangle = \frac{1}{N} \sum_{i=1}^N x_i^n$$

The simulations are performed on UNC's Longleaf computing cluster using 200 processors. The computation takes approximately 8 hours to perform  $4 * 10^5$  timesteps needed to resolve the flow and reach the diffusion timescale,  $L^2/(\pi^2 \kappa)$ 

Additionally, we utilize the Fourier spectral method to solve the 2D advectiondiffusion equation with Ferry wave shear flow. The computation domain is  $[-H, H] \times$ [0, L]. When H is large enough, we can assume there is a periodic boundary condition in the horizontal direction. Since there are non-penetration conditions in the y-direction, we perform the even extension in the y direction to obtain the periodic condition on the extended domain. Thus, we solve the advection-diffusion equation with periodic boundary conditions on the rectanglular domain  $[-H, H] \times [0, 2L]$ . It can be solved by the standard Fourier spectral method. The time integrator is the 4th-order Runge-Kutta method. In the dealiasing process at each time step, we apply the all-or-nothing filter with the two-thirds rule to the spectrum; that is, we set the upper one-third of the resolved spectrum to zero. We solve the equation with the parameters H = 16, L = 0.2, and time increment  $\Delta t = 0.005$  over 2000 timesteps. The grid resolution is  $2048 \times 257$  before the even extension and  $2048 \times 512$  after the extension.

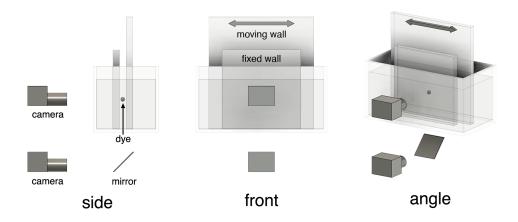


FIG. 2. Schematic showing the experimental setup.

4. Experimental methods. Experiments were performed in a 50x25x30 cm glass tank filled with sodium chloride solution. The fluid was density stratified using the two bucket method to reduce effects of thermal convection. The density of the background fluid linearly decreases with height, with total variation 0.1 g/cc over 20 cm. Two plexiglass walls of 0.125 in thickness are supported vertically using 3d-printed guides glued to the bottom of the tank. Guides were also 3d-printed to maintain the gap thickness between the top of the walls. One wall is connected from above to a linear stage driven by an Oriental motor model ARM66MC with driver model ARD-A, which translates the wall in the horizontal direction parallel to the fixed wall. The motor is controlled by custom software written in MATLAB for the ATMEL ATMEGA2560 microcontroller and implemented using an Arduino MEGA 2560. To prepare the tracer, fluorescein powder is mixed with saline solution of density 1.05 g/cc to a concentration of 0.8 g/L. About 1 mL of fluorescein solution is injected between the walls near the center of the interrogation region. The tank and motor frame are draped in black fabric to block ambient light, and a blacklight is placed on top of the tank to illuminate the tracer. The illuminated fluorescein dye is photographed from the side using a Nikon D300, typically in 4 second intervals over the course of 8 hours. A first-surface mirror tilted back 45 degrees from vertical is placed below the tank to allow for easily viewing the dye from below. To process the dye images, a background intensity value is subtracted, and the intensity distribution is normalized over the viewing area. To capture particle tracking velocimetry (PTV) images, saline solution of density 1.05 g/cc is mixed with 50 micron diameter hollow glass microspheres and injected into the interrogation region. A laser sheet with normal in the vertical direction illuminates the fluid which is viewed from below using 30 fps video captured on a Nikon D750 equipped with a Nikon AF-S micro Nikkor 105 mm lens. PTV processing is performed in MATLAB using PTVlab [Brevis]. Figure 2 shows a schematic of the experimental setup from three different views. [9].

5. Experimental and theoretical results. Here we present a comparison of experimental results with the theory developed above as well as Monte-Carlo and pseudo-spectral simulations for the evolving passive scalar field. First, in figure 3 we show an experimental and theoretical comparison between the Ferry wave velocity distribution (2.7) for two different cases corresponding to two different amplitude wall

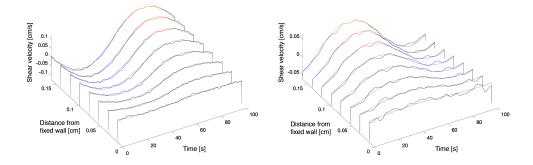


FIG. 3. Comparison of Particle Tracking Velocimetry (PTV) data with the Ferry wave analytical solution. Each slice corresponds with a time series of the shear velocity over a duration of one period taken at different distances between the fixed wall and the moving wall (located at L = 0.16 cm). Left panel has wall oscillation amplitude A = 2 cm, right panel has A = 1 cm, other parameters:  $\omega = 2\pi * 0.01/s, \nu = 0.0113$  poise, and L = 0.16 cm

motions. The left panels show the shear velocity time series at 8 different locations uniformly distribute across the channel for a case with A = 2 cm,  $\omega = 2\pi * 0.01/s$ ,  $\nu = 0.0113$  poise, and L = 0.16 cm, while the right panels change the amplitude to A = 1 cm.

Next, in figure 4 we show the experimental and Monte-Carlo simulations for the dye distribution viewed from the side at times t = 0 s, t = 7200 s, and t =14,400 s for the parameters run in the right panels of figure 3, with smaller wall oscillation amplitude, 1cm, using the experimentally measured value of the diffusivity of Fluorescein in salt water of  $\kappa = 3.3 * 10^{-6} \text{ cm}^2/s$ . Note that in the absence of the wall motion, the cloud would have only spread  $\sqrt{2\kappa t} = 0.3$  cm. In the case with A = 1 cm, the enhanced diffusivity is 19.3 times that of the bare diffusivity, while with A = 2 cm the magnification value is 74.1 shown in figure 5 is the experimenately measured centered variance corresponding to the case with wall oscillation amplitude, 1 cm, along with the best linear fit, and theoretically computed long time behavior of the centered second moment.

We can gain some insight into the transient effects giving rise to the long time limiting effective diffusion by studying the short time behavior using the spectral method with different diffusivities. Shown in figure 6 are images of the scalar distributions, each case output at 5 different times taken on quarter cycles of the wall oscillation. The top cases correspond to a pure time-varying linear shear with a single frequency cosine wall motion, while the bottom panels correspond to cases with a nonlinear Ferry wave, with parameters  $\nu = 0.001$  poise,  $\omega = 0.2\pi/s$ , L = 0.2 cm, A = 1 cm. The left panels have zero diffusivity, while the right panels have  $\kappa = 10^{-5} \text{ cm}^2/\text{s}$ . Observe in the case of the Ferry wave, the scalar is stretched into an extremely thin filament in the upper part of the channel which diffuses rapidly in the non-zero diffusivity case. Compared to the linear shear, this case diffuses faster locally in the upper channel. The case with linear shear is more uniformly mixed across the channel. In the nonlinear Ferry wave case, the upper channel mixes very quickly. This in turn increases the vertical concentration gradient, which gives rise to increased transient vertical diffusive tracer mixing. This effect is perhaps more pronounced than in the more familiar steady pressure driven flow as a full cycle returns the Lagrangian map to its initial configuration.



(a)

t = 0 hrs t = 2 hrs t = 4 hrs(b)

(0)

FIG. 4. Experimental and Monte-Carlo simulation comparison of dye distributions viewed from the side at times t = 0, 2, 4 hours, with parameters corresponding to figure 3, (a): wall oscillation amplitude A = 2 cm, (b): A = 1 cm.

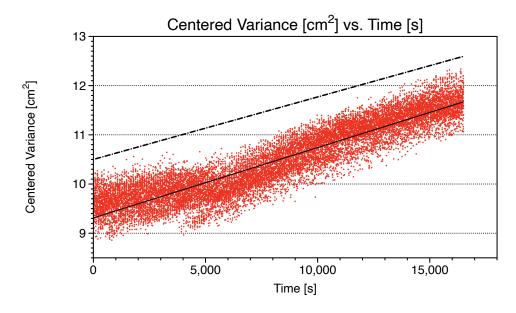


FIG. 5. Evolution of centered scalar variance for experiment along with best linear fit (solid), and theoretical limiting effective diffusion line for the case with wall oscillation amplitude A = 1 cm.

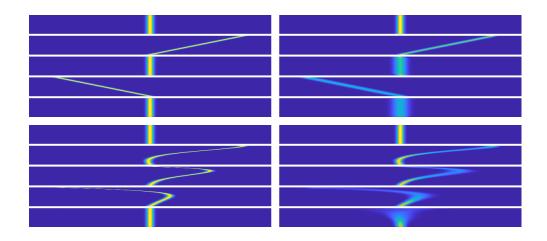


FIG. 6. Spectral method comparison between mixing by linear shear versus nonlinear Ferry wave with a single frequency sinusoidal wall motion. Upper panels correspond to linear shear, while the lower panels correspond to the nonlinear Ferry wave, with parameters  $\nu = 0.001$  poise,  $\omega = 0.2\pi$  /s, L = 0.2 cm, A = 1 cm. The left panels are computed with  $\kappa = 0$  cm<sup>2</sup>/s, while the right panels utilize  $\kappa = 10^{-5}$  cm<sup>2</sup>/s. Output times are taken at quarter periods.

These are the physical mechanisms which give rise to the very different enhanced diffusivities for these two cases: for the linear shear case,  $\kappa_{eff} = 0.00013 \text{ cm}^2/\text{s}$ , 13 times the bare molecular diffusivity. This value is nearly the upper bound for linear shear described above, which in this case is 13.5 the molecular diffusivity. On the other hand, in the nonlinear Ferry wave case,  $\kappa_{eff} = 0.00042 \text{ cm}^2/\text{s}$ , which is 42 times the bare molecular diffusivity.

We next examine the skewness behavior for a nonlinear Ferry wave with parameters  $\nu = 0.01$  poise,  $\omega = 0.2\pi/\text{s}$ , L = 0.2 cm, A = 1 cm, and  $\kappa = 5 * 10^{-6} \text{ cm}^2/\text{s}$  and document how its sign can be controlled the initial phase of sinusoidal wall motion. The initial function is a symmetric function  $f(x, y) = \frac{\exp\left(-\frac{1}{2}\left(\frac{x}{\sigma}\right)^2\right)}{\sqrt{2\pi\sigma}}$  and  $\sigma = \frac{1}{2}$ . Shown in figure 7 are the evolution of the total skewness as the phase of the wall motion is changed computed using Monte-Carlo simulations. Clearly the skewness shows rapid oscillation on these timescales, and the phase clearly can be used to adjust the sign of the skewness. Lastly, in figure 8 we show the short time comparison of the Geometric skewness derived in the absence of diffusion with that computed with diffusion via Monte-Carlo simulations.

6. Conclusions. In this paper we have documented how a transversely moving wall can produce greatly enhanced mixing of a solute in a Newtonian fluid. Experiments compare favorably with the theory and computations. Further, a new mixing mechanism is identified distinguishing linear shear from the nonlinear Ferry wave. A bound for the enhanced diffusion for the linear case is derived and shown to solely depend on the aspect ratio and molecular diffusivity, whereas for the nonlinear Ferry wave occurring at finite viscosity, the enhanced diffusion is unbounded in increasing frequency. Moreover, the enhanced diffusion for the nonlinear Ferry wave possesses a maximum as a function of the viscosity. Lastly, we document how the phase of the wall motion can be used to control the sign of the skewness, whereas we prove the linear shear has zero total skewness for all time. Future directions we intend to explore include utilizing lubrication theory to assess the role of non-planar wall motions

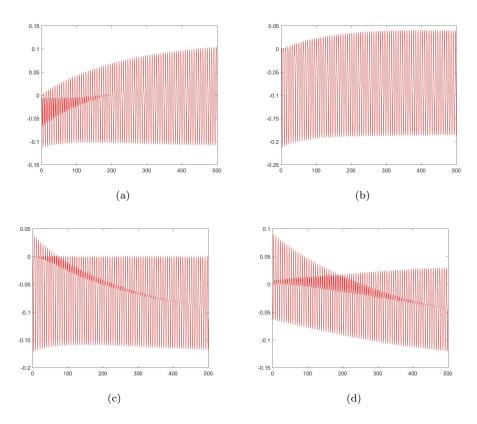


FIG. 7. Skewness arising from wall motions  $\sin(\omega(t+s))$  started at different phase s. a s = 0,  $b \ s = \frac{\pi}{4}$ ,  $c \ s = \frac{\pi}{2}$ ,  $d \ \frac{3\pi}{4}$ , for the nonlinear Ferry wave with parameters  $\nu = 0.01$  poise,  $\omega = 0.2\pi/s$ ,  $L = 0.2 \ cm$ ,  $A = 1 \ cm$ , and  $\kappa = 5 * 10^{-6} \ cm^2/s$ .

and their ability to further increase the effective diffusivity, along with pushing the wall motion into the stochastic regime to further understand how random wall motion creates intermittency in a passive scalar [12].

Acknowledgement. We acknowledge funding received from the following NSF Grant Nos.: DMS-1517879, and DMS-1910824; and ONR Grant No: ONR N00014-18-1-2490.

## 7. Appendix.

**7.1. Multiscale calculation.** Following the prior work [14], we utilize multiplescale analysis below (here in non-dimensional form) to derive the effective diffusion equation at long time induced by the time-varying shear flow. Consider the following advection-diffusion equation:

(7.1) 
$$\begin{array}{c} \frac{\partial T}{\partial t} + v(y,t)\frac{\partial T}{\partial x} = -\kappa\Delta T\\ T|_{t=0} = -\delta(\frac{x}{a}) \end{array}$$

Let  $x' = \frac{x}{a}, y' = \frac{y}{L}, t' = \frac{\epsilon^2 \kappa}{L^2} t, Pe = \frac{LU}{\kappa}, v'(y', \frac{t'}{\epsilon^2}) = \frac{v(Ly', \frac{L^2}{\epsilon^{2\kappa}}t')}{U}, \epsilon = \frac{L}{a} \ll 1$ . We have

(7.2) 
$$\frac{\frac{\partial T}{\partial t'} + \frac{Pe}{\epsilon}v'(y', \frac{t'}{\epsilon^2})\frac{\partial T}{\partial x'} = \frac{\partial^2 T}{\partial x'^2} + \frac{1}{\epsilon^2}\frac{\partial^2 T}{\partial y'^2}}{T|_{t=0}} = \delta(x')$$

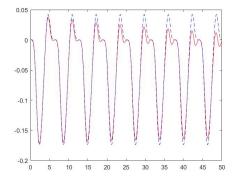


FIG. 8. Comparison of short time skewness (solid red) with analytically predicted short time asymptotic Geometric skewness (dashed blue) arising from wall motions  $\sin(\omega(t + s))$  started at phase  $s = \frac{\pi}{2}$ , for the nonlinear Ferry wave with parameters  $\nu = 0.01$  poise,  $\omega = 0.2\pi/s$ , L = 0.2 cm, A = 1 cm, and  $\kappa = 5 * 10^{-6}$  cm<sup>2</sup>/s

We can drop the primes without confusion and obtain the non-dimensionalized equation

(7.3) 
$$\frac{\partial T}{\partial t} + \frac{Pe}{\epsilon}v(y, \frac{t}{\epsilon^2})\frac{\partial T}{\partial x} = \frac{\partial^2 T}{\partial x^2} + \frac{1}{\epsilon^2}\frac{\partial^2 T}{\partial y^2}$$
$$T|_{t=0} = \delta(x)$$

We seek the asymptotic approximation to T(x, y, t) in the limit  $\epsilon \to 0$  that has the following multiscale expansion

(7.4) 
$$T(x, y, t) = T_0(x, y, t) + \epsilon T_1(x, y, t) + \epsilon^2 T_2(x, y, t) + O(\epsilon^3)$$

We introduce the two extra variables  $\xi = \frac{x}{\epsilon}, \tau = \frac{t}{\epsilon^2}$ . Consequently, the differential operators along the x and t-direction will be replaced

(7.5) 
$$\frac{\frac{\partial}{\partial x} \to \frac{\partial}{\partial x} + \frac{1}{\epsilon} \frac{\partial}{\partial \xi}}{\frac{\partial}{\partial t} \to \frac{\partial}{\partial t} + \frac{1}{\epsilon^2} \frac{\partial}{\partial \tau}}, \quad \frac{\partial^2}{\partial x^2} \to \frac{\partial^2}{\partial x^2} + \frac{2}{\epsilon} \frac{\partial^2}{\partial x \partial \xi} + \frac{1}{\epsilon^2} \frac{\partial^2}{\partial \xi^2}$$

We would have a hierarchy of equations, as one would see in a classical homogenization problem, such that the following equation holds for arbitrarily small  $\epsilon$ .  $O(\epsilon^{-2})$ , we have

(7.6) 
$$LT_0 = 0 T_0(x,\xi,y,t,\tau)|_{t=0,\tau=0} = T_0(x)$$

where  $LT = \left(\frac{\partial}{\partial \tau} + Pev(y,\tau)\frac{\partial}{\partial \xi} - \frac{\partial^2}{\partial \xi^2} - \frac{\partial^2}{\partial y^2}\right)T$ . Since the initial condition is a function of variable x only, we have  $T_0(x,\xi,y,t,\tau) = T_0(x,t)$ .

 $O(\epsilon^{-1}),$ 

(7.7) 
$$LT_1 = -Pev(y,\tau)\frac{\partial T_0}{\partial x} + 2\frac{\partial^2 T_0}{\partial x \partial \xi}$$
$$T_1(x,0) = 0$$

The last term on the right hand side is zero. The solvability condition is guaranteed by  $\langle -Pev(y,\tau)\frac{\partial T_0}{\partial x}\rangle = 0$ , where  $\langle f(y,\tau)\rangle = \lim_{T\to\infty} \frac{1}{T} \int_0^T \int_0^T f(y,\tau) dy d\tau$ . The general form 13 of the solution is  $T_1 = \frac{\partial T_0}{\partial x}(x,t)\theta(\xi,y,\tau) + C(x,t)$ . Therefor, we have

(7.8) 
$$L\theta = -Pev \\ \theta_y|_{y=0} = \theta_y|_{y=1} = 0 \\ \theta(\xi, y, 0) = 0$$

Since the initial condition and the driver independent on  $\xi$ , we have  $\theta(\xi, y, \tau) = \theta(t, \tau)$ .  $O(\epsilon^0)$ 

(7.9) 
$$\frac{\partial T_2}{\partial \tau} + LT_2 = -\frac{\partial T_0}{\partial t} - Pev(y, \frac{t}{\epsilon^2})\frac{\partial T_1}{\partial x} + \frac{\partial^2 T_0}{\partial x^2} + 2\frac{\partial^2 T_1}{\partial x\partial \xi}$$
$$T_2(x, 0) = 0$$

Since  $\theta$  independent on  $\xi$ , the last term on the right hand side is zero. The solvability condition yields the effective diffusion equation

(7.10) 
$$-\frac{\partial T_0}{\partial t} + \kappa_{eff} \frac{\partial^2 T_0}{\partial x^2} = 0$$

where  $\kappa_{eff} = 1 - Pe \langle v(y, \tau)\theta \rangle$  is the effective diffusivity. With comparing equation (7.12) and (2.9), we can see that the solution  $\theta$  of the cell problem is the first Aris moment  $T_1$ . The formula of effective diffusivity (7.10) is equivalent to effective diffusivity defined by the leading order of the cross-sectional average of the Aris moments  $\langle T_2 \rangle$ . Hence, we conclude that Aris moment approach and the multiscale analysis approach yield the same effective diffusivity for any time-varying shear flow.

Let's use the linear shear flow as an example. Let  $\omega' = \omega \frac{L^2}{\kappa}, U = A\omega$ , we have

(7.11) 
$$v' = \frac{u}{U} = y' \sin \omega' \frac{t'}{\epsilon^2}$$

Equation (7.12) becomes

(7.12) 
$$\begin{aligned} \frac{\partial \theta}{\partial \tau} - \frac{\partial^2 \theta}{\partial y^2} &= -Pey \sin \omega t\\ \theta_y|_{y=0} &= \theta_y|_{y=1} = 0\\ \theta(y,0) &= 0 \end{aligned}$$

By series expansion, we have

(7.13) 
$$\theta = \frac{\Pr(\cos(t\omega) - 1)}{2\omega} + \sum_{i \in odd} \frac{4\Pr\left(\omega e^{\pi^2 \left(-i^2\right)t} + \pi^2 i^2 \sin(t\omega) - \omega \cos(t\omega)\right)}{\pi^2 i^2 (\pi^4 i^4 + \omega^2)} \cos i\pi y$$

By formula (7.10), the effective diffusivity is

(7.14)  

$$\begin{aligned} \kappa_{eff} &= 1 + \sum_{i \in odd} \frac{4 \operatorname{Pe}^2 \omega}{\pi^2 i^2 (\pi^4 i^4 \omega + \omega^3)} \\ &= 1 + \frac{\operatorname{Pe}^2}{2\omega^2} - \frac{\operatorname{Pe}^2 \left( \sin\left(\frac{\sqrt{\omega}}{\sqrt{2}}\right) + \sinh\left(\frac{\sqrt{\omega}}{\sqrt{2}}\right) \right)}{\sqrt{2}\omega^{5/2} \left( \cos\left(\frac{\sqrt{\omega}}{\sqrt{2}}\right) + \cosh\left(\frac{\sqrt{\omega}}{\sqrt{2}}\right) \right)} \end{aligned}$$

This is the non-dimensionalized version of the effective diffusivity in the formula (2.14).

**7.2. The Ferry wave in three dimensional space.** For completeness we can also derive the fluid flow for a Ferry wave in an infinitely long rectangular duct  $y \times z \in [0, L] \times [0, a]$ . In this case, the flow satisfies the equation:

(7.15) 
$$\begin{aligned} u_t &= \nu(u_{yy} + u_{zz}) \\ u(0, z, t) &= 0, \quad u(L, z, t) = f(t) \quad u(y, z, 0)|_{\partial\Omega} = 0 \\ 14 \end{aligned}$$

Applying Laplace transform yields

(7.16) 
$$\begin{aligned} \hat{su} &= \nu(\hat{u}_{yy} + \hat{u}_{zz}) \\ \hat{u}(y, 0, s) &= 0 \quad \hat{u}(y, 1, t) = \hat{f}(t) \end{aligned}$$

Let  $f(t) = A\omega \cos \omega t$ , so  $\hat{f}(s) = \frac{A\omega s}{s^2 + \omega^2}$ . We assume the solution takes the form

(7.17) 
$$\hat{u} = \sum_{i=1}^{\infty} \sin\left(\frac{iz\pi}{a}\right) f_i(y,s)$$

Substitute (7.17) into (7.16) leads to

(7.18)  

$$s\sum_{i=1}^{\infty}\sin\left(\frac{iz\pi}{a}\right)f_i(y,s) = \nu\left(\sum_{i=1}^{\infty} - \left(\frac{i\pi}{a}\right)^2\sin\left(\frac{iz\pi}{a}\right)f_i(y,s) + \sum_{i=1}^{\infty}\sin\left(\frac{iz\pi}{a}\right)\frac{\partial^2}{\partial y^2}f_i(y,s)\right)$$

Hence  $f_i(y, s)$  satisfies the equation

(7.19) 
$$\left(\nu\left(\frac{i\pi}{L}\right)^2 + s\right)f_i(y,s) = \nu\frac{\partial^2}{\partial y^2}f_i(y,s)$$

With the boundary condition  $f_i(0,s) = 0$ , we have  $f_i(y,s) = c_i \sinh\left(\frac{y\sqrt{\pi^2 i^2 \nu + a^2 s}}{a}\right)$ . The coefficients  $c_i$  can be determined by the boundary condition  $\hat{u}(L,z,s) = \frac{A\omega s}{s^2 + \omega^2}$  and the orthogonality of  $\sin\left(\frac{iz\pi}{a}\right)$ ,

(7.20) 
$$c_i = \frac{4As\omega}{\pi i (s^2 + \omega^2) \sinh\left(\frac{L\sqrt{\pi^2 i^2 \nu + a^2 s}}{a}\right)} \quad i \in \text{odd}$$

Hence the  $\hat{u}$  is

(7.21) 
$$\hat{u} = \sum_{i \in odd}^{\infty} \frac{4As\omega}{\pi i (s^2 + \omega^2) \sinh\left(\frac{L\sqrt{\pi^2 i^2 \nu + a^2 s}}{a}\right)} \sinh\left(\frac{L\sqrt{\pi^2 i^2 \nu + a^2 s}}{a}\right) \sin\left(\frac{iz\pi}{a}\right)$$

The poles of  $\hat{u}$  are  $\pm i\omega$  and  $-\frac{\pi^2(i^2\nu+a^2n^2)}{a^2}$ . By inverse Laplace transformation and residue theorem, we have the solution of equation (7.15) (7.22)

$$\begin{aligned} u &= \sum_{i \in odd} \frac{2A\omega}{\pi i} \left( e^{it\omega} \sin\left(\frac{\pi iz}{a}\right) \operatorname{csch}\left(\frac{L\sqrt{\pi^2 i^2 \nu + ia^2 \omega}}{a}\right) \sinh\left(\frac{y\sqrt{\pi^2 i^2 \nu + ia^2 \omega}}{a}\right) \\ &+ e^{-it\omega} \sin\left(\frac{\pi iz}{a}\right) \operatorname{csch}\left(\frac{L\sqrt{\pi^2 i^2 \nu - ia^2 \omega}}{a}\right) \sinh\left(\frac{y\sqrt{\pi^2 i^2 \nu - ia^2 \omega}}{a}\right) \right) + O\left(e^{-\frac{t\pi^2\left(\nu + a^2\right)}{a^2}}\right) \end{aligned}$$

## REFERENCES

- A. Ajdari, N. Bontoux, and H. A. Stone. Hydrodynamic dispersion in shallow microchannels: the effect of cross-sectional shape. *Analytical Chemistry*, 78(2):387–392, 2006.
- [2] M. Aminian, F. Bernardi, R. Camassa, D. M. Harris, and R. M. McLaughlin. How boundaries shape chemical delivery in microfluidics. *Science*, 354(6317):1252–1256, 2016.
- [3] M. Aminian, F. Bernardi, R. Camassa, and R. M. McLaughlin. Squaring the circle: Geometric skewness and symmetry breaking for passive scalar transport in ducts and pipes. *Physical review letters*, 115(15):154503, 2015.
- [4] R. Aris. On the dispersion of a solute in a fluid flowing through a tube. Proceedings of the Royal Society of London. Series A. Mathematical and Physical Sciences, 235(1200):67–77, 1956.

- M. Avellaneda and A. J. Majda. Stieltjes integral representation and effective diffusivity bounds for turbulent transport. *Physical review letters*, 62(7):753, 1989.
- [6] M. Avellaneda and A. J. Majda. Mathematical models with exact renormalization for turbulent transport. Communications in mathematical physics, 131(2):381–429, 1990.
- [7] M. Avellaneda and A. J. Majda. Renormalization theory for eddy diffusivity in turbulent transport. *Physical review letters*, 68(20):3028, 1992.
- [8] M. Avellaneda and A. J. Majda. Superdiffusion in nearly stratified flows. Journal of statistical physics, 69(3-4):689–729, 1992.
- W. Brevis, Y. Niño, and G. Jirka. Integrating cross-correlation and relaxation algorithms for particle tracking velocimetry. *Experiments in Fluids*, 50(1):135–147, 2011.
- [10] J. C. Bronski and R. M. McLaughlin. The problem of moments and the majda model for scalar intermittency. *Physics Letters A*, 265(4):257–263, 2000.
- [11] J. C. Bronski and R. M. McLaughlin. Rigorous estimates of the tails of the probability distribution function for the random linear shear model. *Journal of Statistical Physics*, 98(3-4):897–915, 2000.
- [12] R. Camassa, Z. Kilic, and R. M. McLaughlin. On the symmetry properties of a random passive scalar with and without boundaries, and their connection between hot and cold states. *Physica D: Nonlinear Phenomena*, 400:132124, 2019.
- [13] R. Camassa, Z. Lin, and R. M. McLaughlin. Evolution of the probability measure for the majda model: New invariant measures and breathing pdfs. *Journal of Statistical Physics*, 130(2):343–371, 2008.
- [14] R. Camassa, Z. Lin, and R. M. McLaughlin. The exact evolution of the scalar variance in pipe and channel flow. *Communications in Mathematical Sciences*, 8(2):601–626, 2010.
- [15] J. D. Ferry, W. Sawyer, and J. Ashworth. Behavior of concentrated polymer solutions under periodic stresses. *Journal of Polymer Science*, 2(6):593–611, 1947.
- [16] A. J. Majda. The random uniform shear layer: an explicit example of turbulent diffusion with broad tail probability distributions. *Physics of Fluids A: Fluid Dynamics*, 5(8):1963–1970, 1993.
- [17] A. J. Majda and R. M. McLaughlin. The effect of mean flows on enhanced diffusivity in transport by incompressible periodic velocity fields. *Studies in applied mathematics*, 89(3):245– 279, 1993.
- [18] R. M. McLaughlin and A. J. Majda. An explicit example with non-gaussian probability distribution for nontrivial scalar mean and fluctuation. *Physics of Fluids*, 8(2):536–547, 1996.
- [19] S. M. Mitran, M. G. Forest, L. Yao, B. Lindley, and D. B. Hill. Extensions of the ferry shear wave model for active linear and nonlinear microrheology. *Journal of non-Newtonian fluid* mechanics, 154(2-3):120–135, 2008.
- [20] H. A. Stone, A. D. Stroock, and A. Ajdari. Engineering flows in small devices: microfluidics toward a lab-on-a-chip. Annu. Rev. Fluid Mech., 36:381–411, 2004.
- [21] G. I. Taylor. Dispersion of soluble matter in solvent flowing slowly through a tube. Proceedings of the Royal Society of London. Series A. Mathematical and Physical Sciences, 219(1137):186-203, 1953.
- [22] E. Vanden Eijnden. Non-gaussian invariant measures for the majda model of decaying turbulent transport. Communications on Pure and Applied Mathematics: A Journal Issued by the Courant Institute of Mathematical Sciences, 54(9):1146–1167, 2001.
- [23] S. Vedel, E. Hovad, and H. Bruus. Time-dependent taylor-aris dispersion of an initial point concentration. Journal of fluid mechanics, 752:107–122, 2014.